03,13

# Interface doping of zinc oxide nanorods

© A.A. Ryabko[1], D.S. Mazing[2], A.A. Bobkov[2], A.I. Maximov[2], V.S. Levitskii[1], E.F. Lazneva[3], A.S. Komolov[3], V.A. Moshnikov[2], E.I. Terukov[1]

[1] Ioffe Institute,
St. Petersburg, Russia
[2] St. Petersburg State Electrotechnical University „LETI",
St. Petersburg, Russia
[3] St. Petersburg State University,
St. Petersburg, Russia

E-mail: a.a.ryabko93@yandex.ru

*Received June 16, 2022*
*Revised June 16, 2022*
*Accepted June 18, 2022*

The effect of an increase in the electrical conductivity of a system of zinc oxide nanorods by a factor of $10^5$ during atomic layer deposition of a thin dielectric layer of aluminum oxide was found. It is shown that a change in the electrical conductivity of zinc oxide during atomic layer deposition of aluminum oxide on the surface is also observed for thin polycrystalline layers of zinc oxide. A study of polycrystalline layers of zinc oxide coated with aluminum oxide using ultraviolet and X-ray photoelectron spectroscopy is presented. Based on the results of photoelectron spectroscopy, two main factors for changing the electrical conductivity are proposed, which consist in the formation of a two-dimensional electron gas at the $ZnO|Al_2O_3$ interface and doping of the near-surface region of zinc oxide with aluminum atoms.

**Keywords:** nanorods, zinc oxide, aluminum oxide, atomic layer deposition, transparent electrodes, X-ray photoelectron spectroscopy, ultraviolet photoelectron spectroscopy.

DOI: 10.21883/PSS.2022.11.54187.408

## 1. Introduction

Zinc oxide ZnO is a direct band gap *n*-type semiconductor with a band gap of $E_g \approx 3.3$ eV. ZnO is characterized by ion-covalent bonds, at normal conditions it crystalizes in the wurtzite structure. This is responsible for piezoelectric properties of ZnO. The electron type of ZnO conductivity without doping is associated with its intrinsic point defects, predominantly vacancies of oxygen and Zn interstitials [1]. Undoped layers of ZnO are used as a transparent electron-transport layer in photovoltaic structures [2–4]. Doping of ZnO with Al or Ga atoms provides for the use of ZnO layers as transparent conductive electrodes [5–8]. ZnO is attractive for the creation of emitters and detectors in the near ultraviolet range, such as LEDs, lasers, and photodiodes [9–11]. However, currently the difficulty of forming a $p-n$-junction in ZnO with pre-defined properties impedes the creation of high-quality diode structures.

The most interesting for researchers is ZnO in the form of different 0D, 1D, 2D, and 3D nanomaterials. At the same time 1D-nanoobjects of ZnO are the most widely used in studies.

Thanks to fast-growing (0001), $(000\bar{1})$ polar surfaces, ZnO can be easily formed as nanorods by methods of gas-phase and hydrothermal synthesis. Single-crystal nanorods of ZnO are studied for applications in optoelectronics and nanophotonics [12,13], photocatalysis [14], piezoelectric nanogenerators [14], and photocatalysts [15]. Due to high mobility of electrons, good chemical and thermal stability ZnO nanorods have come into sharp focus as a gas sensor material [16–19]

In the field of photovoltaic structures ZnO nanorod arrays are attractive for the creation of an ordered bulk heterojunction with a light-absorbing semiconductor. The bulk heterojunction should ensure an increase in current of the photovoltaic structure due to the increase in the specific area of the heterojunction and increase in the effective thickness of the absorbing material [13]. Mesoscopic nanostructured photoelectrodes allow photovoltaic cells working in conditions of low and dissipated solar radiation in a more effective manner than photovoltaic cells with the planar structure [20]. At the same time, in contrast to layers of nanoparticles, nanorods provide for the transport of charge carriers to the electrode without scattering on grain boundaries.

However, today the use of ZnO in the form of nanorods in photovoltaic structures, in particular, solar cells based on colloidal quantum dots, does not result in efficiency improvement as compared with planar structures. This is associated with the increase in charge carrier recombination on the superficial defects of ZnO nanorods due to a large area of the interphase boundary ZnO|colloidal quantum dots. This reduces the no-load voltage of the structure [21].

One of approaches to passivate surface defects of ZnO nanorods is to apply thin layers of other materials onto ZnO [21,22]. Often, to passivate surface defects of ZnO,

thin tunnel-transparent dielectric layers of $Al_2O_3$ aluminum oxide are applied [23–25], that are widely used to passivate the silicon surface [26–28]. A method of conform and precise coating of objects with aluminum oxide is atomic layer deposition (ALD) [29]. Concurrently with this, in the scientific literature an approach is presented to form ZnO doped with aluminum, ZnO : Al, using the atomic layer deposition, where cycles of $Al_2O_3$ deposition are included in cycles of ZnO deposition [8,30,31].

In this study we considered the effect of deposition of thin dielectric layer of $Al_2O_3$ onto ZnO nanorods and films.

## 2. Materials and research techniques

The formation of coating of ZnO nanorods consisted in the deposition of a thin seed layer and growth of nanorods from seed centers. The nanorods were synthesized by a low-temperature hydrothermal method with the suppression of nucleation in the bulk solution at a temperature of 85°C. $Zn(NO_3)_2$ zinc nitrate and $(CH_2)_6N_4$ hexamethylenetetramine with equimolar concentration of 25 mM were used as precursors, and nucleation was suppressed by adding $NH_4OH$ ammonium hydroxide and $[-CH_2CH_2NR-]_n$ polyethyleneimine to the solution. The seed layer for the subsequent growth of nanorods was produced by the ultrasonic spray pyrolysis of aqueous solution of $Zn(CH_3CO_2)_2$ zinc acetate with a concentration of 0.05 M. Features of this two-step method to synthesize coatings of ZnO nanorods are described in [32]. After the synthesis, the samples were annealed at a temperature of 500°C for 5 min to remove organic compounds from the surface of the nanorods.

The method of thermal atomic layer deposition was used to deposit thin dielectric layers of $Al_2O_3$ with a thickness of about 5−7 nm (50 cycles) on the nanorod surface. The atomic layer deposition was performed at a temperature of 220°C in the TFS-200 (Beneq) system using $Al_2(CH_3)_6$ trimethylaluminum and deionized water as precursors.

To measure the current flowing through the samples, ZnO nanorod coatings were formed on a ceramic substrate with golden interdigital electrodes (width and distance between electrodes was 25 $\mu$m). Current was recorded by a Keithley 6485 picoammeter with an applied voltage of 5 V. Measurements were carried out in the air atmosphere; prior to the measurements the samples were warmed-up at a temperature of $\sim$ 300°C to desorb water molecules from the nanorod surface. Also, the samples were studied using scanning electron microscopy (SEM) and X-ray photoelectron spectroscopy (XPS).

To study the redistribution of electron density at the atomic layer deposition of $Al_2O_3$ on ZnO, a method of spray pyrolysis was used to produce a series of samples with a thin polycrystalline layer of ZnO, on which $Al_2O_3$ was applied with cycles varied from 0 to 50. A polycrystalline layer of ZnO without $Al_2O_3$ coating and a thin layer of $Al_2O_3$ applied at 50 cycles on the surface of the ZnO layer were studied using ultraviolet photoelectron spectroscopy (UVPS) with a photon excitation energy of $h\nu$(He I) $\approx$ 21.2 eV. A Si-substrate with Pt-coating was used. Both XPS and UVPS of samples were carried out in conditions of ultrahigh-vacuum ($\sim 10^{-7}$ Pa) using an Escalab 250Xi combined photoelectron spectrometer (Thermo Fisher Scientific Inc.), XPS study was performed at photons excitation energy of Al$K_\alpha$ = 1486 eV. XPS-spectra were processed using CasaXPS Version 2.3.24 software. It is known that oxygen- and carbon-containing impurities are actively adsorbed from the air on the surface of metal oxides [33], therefore, prior to measurements the samples with cleaned with $Ar^+$ at 500 V to remove surface adsorbates.

Also, a reference sample was produced with a thickness of $\sim$ 70 nm with 50 cycles of $Al_2O_3$ deposition to measure electrical properties (resistivity, mobility and concentration of charge carriers) using a Hall measurement system (HMS-3000, Ecopia) at a room temperature. The morphology of the reference sample was studied by a method of atomic force microscopy (AFM) using an Integra Terma (NT-MDT) probe nanolaboratory.

## 3. Results and discussion

### 3.1. Morphology of samples and electrical parameters

The morphology of the coating made of ZnO nanorods with a deposited layer of $Al_2O_3$ formed on a ceramic substrate with interdigital electrodes is shown in Fig. 1. In Fig. 1, *a* the graininess of the sample surface can be seen, which is attributable to crystallites of the ceramic substrate. Thus, the growth of nanorods on crystallites of she substrate occurs in different directions (Fig. 1, *a*, insert), that results in an additional concentration of intersection areas of ZnO nanorods (Fig. 1, *b*).

As can be seen from Fig. 1, *b*, the nanorods may considerably differ from each other by width. An increased dispersion of nanorods by width is connected with the roughness of the substrate and the diffusion-limited mode of nanorods growth [32]. A decrease in the distance between the nanorods results in a decrease of their diameters, while the nanorods located on protrusions of the substrate's crystallites have greater diameters. The needle-like shape of the nanorods is typical for synthesis in conditions of lateral growth suppression due to the adsorption of blocking molecules on lateral surfaces [34]. In this case molecules adsorbed on lateral surfaces were those of polyethyleneimine.

Electrical resistance of the coating made of ZnO nanorods on a ceramic substrate with interdigital electrodes before the atomic layer deposition was $\sim$ 5 MΩ (after drying of the sample to remove adsorbed molecules of water). Electrical resistance after the atomic layer deposition of $Al_2O_3$ (with a thickness of about 5−7 nm, 50 cycles of ALD-process) on a coating made of ZnO nanorods was $\sim$ 50 Ω. The process of thermal drying of the sample did not affect the

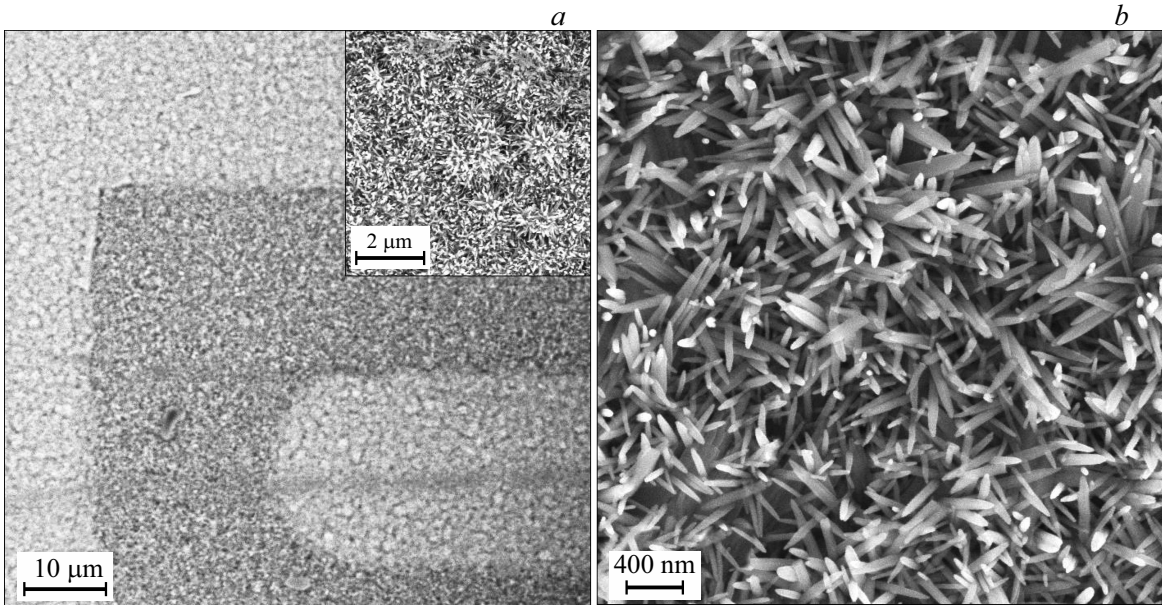


**Figure 1.** SEM-image of ZnO nanorods coated with a thin dielectric layer of $Al_2O_3$, on a ceramic substrate with interdigital electrodes.

resistance significantly. Thus, the atomic layer deposition of the thin dielectric layer of $Al_2O_3$ on the surface of ZnO nanorods resulted in an approximately $10^5$ times increase in the electrical conductivity of the coating made of ZnO nanorods on a ceramic substrate with interdigital electrodes.

Results of XPS for ZnO nanorods before and after the depostion of a thin layer of $Al_2O_3$ (50 cycles of ALD-process) are shown in Fig. 2.

For the ease of comparison the typical intensive peaks of Zn2*p*, O1*s*, C1*s*, Al2*p* on XPS-spectra are moved out of the spectra, while their position is highlighted with a dashed line. Identification of other peaks correspond to [35]. It can be seen from the XPS data, that after the deposition of $Al_2O_3$ (at 50 cycles of ALD-process) no core levels of zinc are observed: aluminum core levels occur instead. An increase in the peak of O1*s* is attributable to the greater content of oxygen in the $Al_2O_3$ compound than in the ZnO. Thus, the atomic layer deposition provides a conformal coating of ZnO nanorods with a thin layer of $Al_2O_3$, which results in a significant increase in their electrical conductivity.

Morphology of the reference sample of $ZnO|Al_2O_3$ with a thickness of $\sim 70$ nm used for measurement of electrical characteristics is shown in Fig. 3.

As can be seen from the AFM-image, the layer of ZnO with $Al_2O_3$ coating is composed of nanocrystallites, while the relief of the layer surface is mainly equal to 10–15 nm. Resistance of ZnO layer measured using golden sure contacts before the application of the $Al_2O_3$ coating was $\sim 1$ GΩ; resistance after the application of $Al_2O_3$ was $\sim 150$ kΩ. Thus, with the use of the ZnO layer, a sharp change in electrical conductivity was also

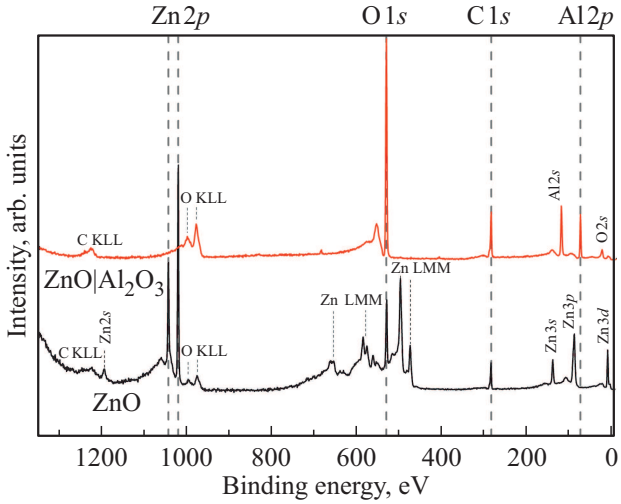


**Figure 2.** Survey XPS-spectra of the coating made of ZnO nanorods before the deposition of $Al_2O_3$ layer and after atomic layer deposition of a thin layer of $Al_2O_3$ (50 cycles of ALD-process). For the substrate of the coating made of ZnO nanorods a silicon substrate was used. Stoichiometric designation of $Al_2O_3$ is conventional. (KLL and LLM are notations of the Auger electrons.)

observed and was $\sim 6.7 \cdot 10^3$. It is evident, that the surface area of the polycrystalline layer is considerably lower than the surface area of the coating made of nanorods of the same weight, that explains the lesser change in the electrical conductivity of the sample. Resistivity of this layer was $4.2 \cdot 10^{-1}\ \Omega \cdot$ cm (concentration of charge carriers is $2.32 \cdot 10^{18}\ \mathrm{cm}^{-3}$, mobility of charge carriers is $2.26\ \mathrm{cm}^2/\mathrm{V} \cdot \mathrm{s}$). We failed to measure the electrical

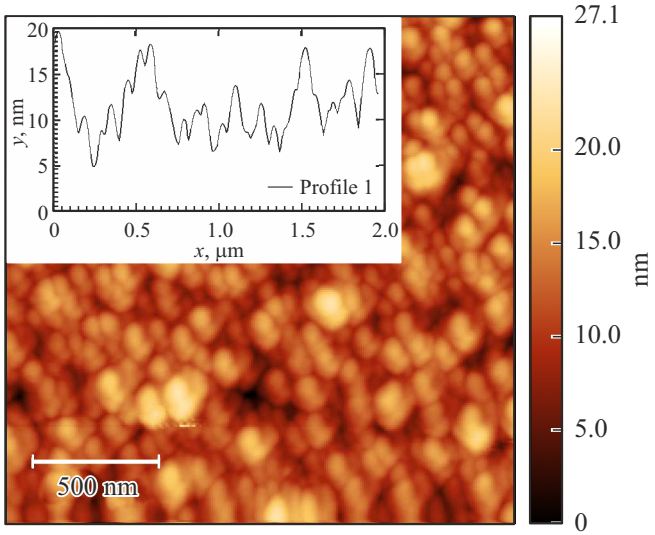


**Figure 3.** AFM-image of the surface of ZnO thin layer coated by $Al_2O_3$ (50 cycles of ALD).

parameters of the layer before the deposition of $Al_2O_3$ layer on ZnO because of too high resistance. These results for resistivity and mobility are comparable with the results for the case of deposition of ZnO films doped with Al by the spray pyrolysis method [36]. But in our study the main contribution to the electrical conductivity is from the near-surface area of the film.

Of course, the resistivity of this layer is significantly higher than the resistivity of transparent conductive oxides, such as indium–tin oxide, tin oxide doped with fluorine, or transparent electrodes based on the doped ZnO, that are produced mainly by the method of magnetron sputtering. However, it is evident, that in the case of ZnO|$Al_2O_3$ nanorods resistivity of ZnO decreases considerably.

### 3.2. Ultraviolet and X-ray photoelectron spectroscopy of ZnO|$Al_2O_3$ coatings

To explain the effect of increase in the electrical conductivity of ZnO upon atomic layer deposition of $Al_2O_3$ on its surface, layers of ZnO before and after the deposition of $Al_2O_3$ were studied using ultraviolet photoelectron spectroscopy (UVPS) and XPS.

UVPS-spectra of the ZnO layer and thin layer of $Al_2O_3$ (50 cycles of ALD) on the ZnO surface are shown in Fig. 4, where boundaries of UVPS-spectra are zoomed to determine values of the cutoff by high binding energy ($E_{cutoff}$) and by onset binding energy ($E_{onset}$).

The width and position of UVPS-spectra for both ZnO and $Al_2O_3$ match well the literature data [37,38]. Also, a typical structure of a valence band is observed on the UVPS-spectrum of ZnO [37]. Work function (Fermi level relative to vacuum) of materials determined by deducting the value of cutoff by high energy (left end of the spectrum, $E_{cutoff}$) from the irradiation energy (21.21 eV) was $A_{ZnO} = 3.8$ eV and $A_{Al_2O_3} = 3.2$ eV. To determine the valence band maximum (VBM) relative to vacuum, the

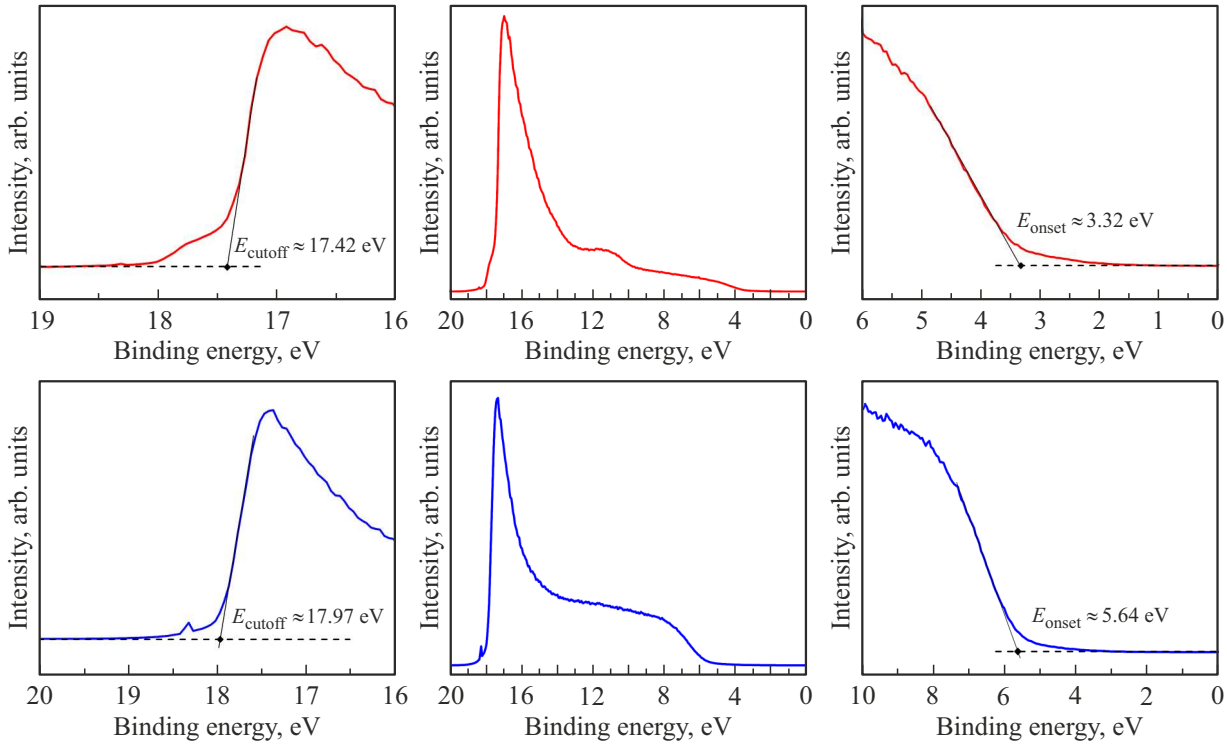


**Figure 4.** UVPS-spectra of ZnO polycrystalline film (top, red line) and $Al_2O_3$ film (50 cycles of ALD) on the surface of ZnO layer.

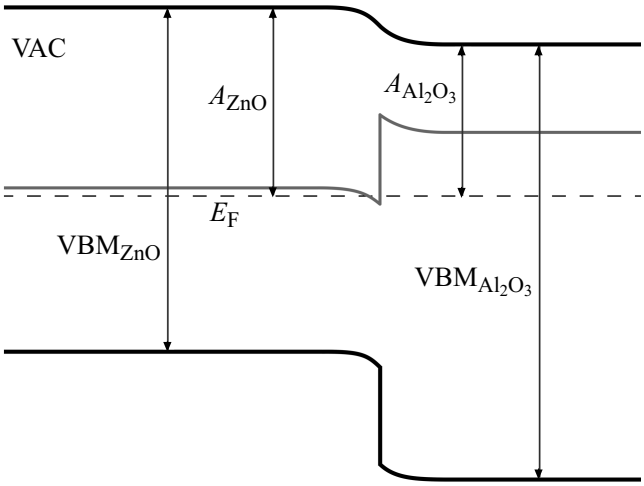


**Figure 5.** Energy band diagram of $ZnO|Al_2O_3$ structure. The bend of $Al_2O_3$ bands attributable to the oxygen ions adsorbed from the atmosphere at the low thickness of the layer was not taken into account in building up the diagram.

work function was added with the value of the onset bond energy ($E_{onset}$, on the right end of the spectrum), i.e. we used the following formula

$$-\text{VBM} = h\nu - (E_{cutoff} - E_{onset}).$$

Positions of valence band maxima relative to vacuum were $VBM_{ZnO} = -7.1$ eV and $VBM_{Al_2O_3} = -8.9$ eV.

To build up the energy band diagram of $ZnO|Al_2O_3$, the position of the conduction band bottom is selected arbitrary. Thus, the width of the ZnO bandgap $E_g = 3.35$ eV was selected to make the bottom of the conduction band slightly higher than the Fermi level. The bandgap width for $Al_2O_3$ was selected equal to 7 eV, which is within the range of the typical bandgap width values (from 6 to 8 eV). The shift of the conduction band bottom of $Al_2O_3$ or ZnO within the range of typical values does not change the characteristic features of the energy band diagram, which is shown in Fig. 5.

As can be seen from the energy band diagram, at the $ZnO|Al_2O_3$ interface a potential well can be formed for

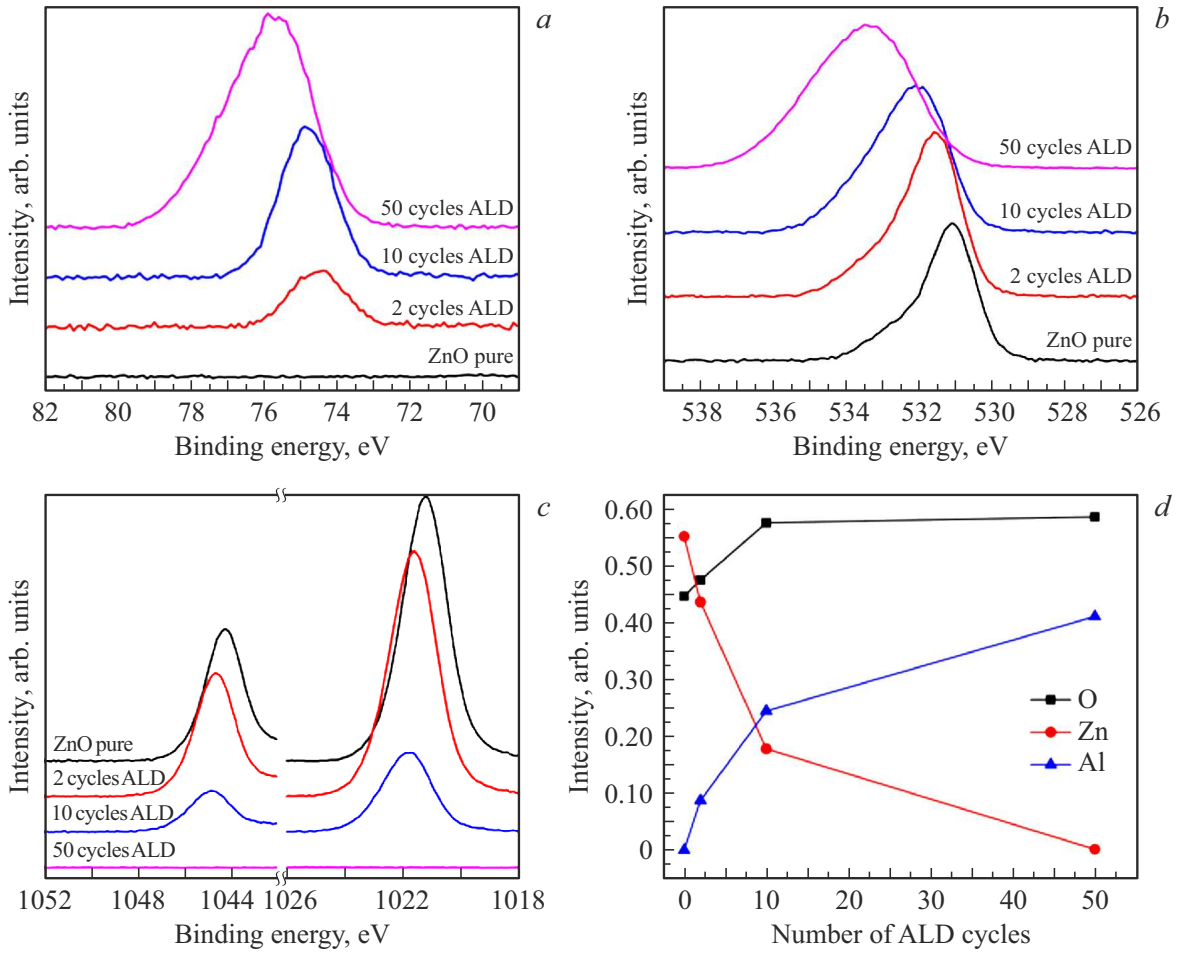


**Figure 6.** Results of XPS for the ZnO layer and the ZnO layer with atomic layer deposition of $Al_2O_3$ with 2, 10, and 50 deposition cycles: *a*) core level Al2*p*, *b*) core level O1*s*, *c*) core level Zn2*p* and *d*) percentage of atoms in the near-surface layer.

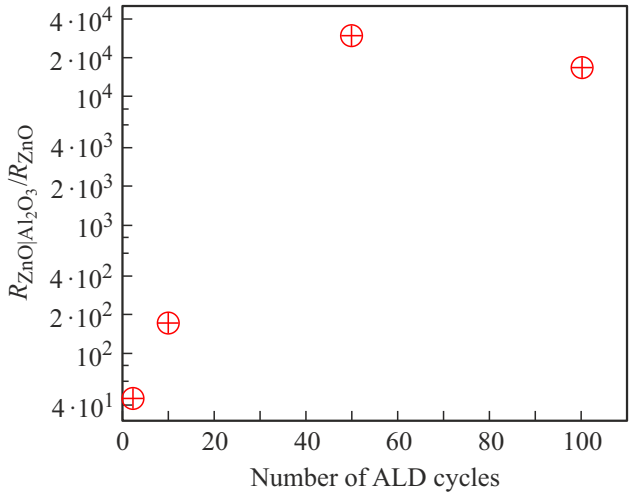


**Figure 7.** Change in resistance of the ZnO layer at the variation of the number of cycles of ALD-process.

electrons, that may be responsible for the observed increase in electrical conductivity.

Results of XPS for ZnO layer with atomic layer deposition of $Al_2O_3$ at 2, 10, and 50 deposition cycles, i.e., core levels Zn2$p$, Al2$p$, O1$s$, as well as percentages of atoms in the near-surface layer are shown in Fig. 6.

As can be seen from Fig. 6, $d$, in the composition of the ZnO near-surface layer before the deposition of $Al_2O_3$ the percentage of Zn atoms relates to the percentage of oxygen atoms in the crystal lattice as 1.2 : 1. High concentration of oxygen vacancies in the ZnO lattice is also typical and is responsible for the $n$-type of electrical conductivity. Deposition of Al atoms on the ZnO surface results in an increase in the ratio of oxygen atoms to metal atoms. At 50 cycles of ALD peaks of core levels Zn2$p$ are almost unobserved, and the ratio of aluminum atoms to oxygen atoms is close to stoichiometric (2 : 3) and equals to 2 : 2.85. The position of peak maximum of O1$s$ (Fig. 6, $b$) in the process of application of the $Al_2O_3$ layer shifts from 530.11 eV for ZnO to 532.45 eV for $Al_2O_3$. What is interesting is the shift of position of core levels Zn2$p$ and Al2$p$. Thus, the peak of Zn2$p_{3/2}$ before the application of $Al_2O_3$ on the surface is at the binding energy of 1021.21 eV, and then it shifts to 1021.60 at two cycles of ALD-process and to 1021.81 eV at ten cycles of ALD-process (Fig. 6, $c$). The position of core level Al2$p$ shifts from 74.55 eV at 2 cycles of ALD-process to values of Al2$p$ for aluminum in a more oxidized form, 74.81 eV at 10 cycles and, finally, 75.74 eV at 50 cycles of ALD-process (Fig. 6, $a$).

The shift of core levels Zn2$p$ of zinc and Al2$p$ of aluminum near the interface (at 2 and 10 cycles of ALD-process) relative to the initial layer of ZnO and the layer at 50 cycles of ALD-process is indicative of their electron interaction and incorporation of Al atoms into the ZnO lattice. Since Al is a typical dopant for ZnO, near-surface doping of ZnO with Al atoms may explain the increase in electrical conductivity as well.

The change in resistance (Fig. 7) measured using golden sure contacts is indicative of the fact that the electrical conductivity of the ZnO layer increases non-linearly with the increase in the number of cycles of ALD-process.

As can be seen from Fig. 7, two cycles of ALD-process result in $\sim 44$ times increase in the conductivity of the ZnO layer, and at ten cycles the resistance decreases $\sim 172$ times. Such a change of electrical conductivity is almost proportional to the change in the number of cycles of ALD-process. However, the increase in the number of cycles up to 50 resulted in a $\sim 3\cdot10^4$-times change in ZnO layer resistance. Further decrease in electrical conductivity with an increase in cycles of ALD-processes may be connected with an increase in the potential barrier between the electrode and the ZnO layer due to the thickness of $Al_2O_3$ dielectric layer.

### 3.3. Discussion of results

The results of studying the ZnO and $Al_2O_3$ on the ZnO surface by UVPS method have shown, that the position of the Fermi level in materials can provide for a potential well to be formed for electrons and, respectively, two-dimensional electron gas to be formed on the interface, that explains the $\sim 10^5$ increase in the electrical conductivity of ZnO nanorods with the deposition of $\sim 5-6$ nm $Al_2O_3$ on their surfaces.

However, the results of measurements of polycrystalline ZnO film resistance with a different number of cycles of $Al_2O_3$ ALD have demonstrated that an increase in electrical conductivity is observed even in the case of low number of cycles of ALD-process (2 and 10 cycles, $\sim 0.2-0.26$ and $\sim 1-1.3$ nm, respectively). At the same time the peak of Al2$p$ in the XPS-spectrum at 2 cycles is shifted from the peak of Al2$p$ at 50 cycles of ALD-process, when the ratio of Al and O becomes close to the stoichiometric composition of the $Al_2O_3$ compound. Also, due to high concentration of oxygen vacancies in the near-surface layer of ZnO (Fig. 6, $d$), oxygen can be trapped when depositing $Al_2O_3$. Therefore, it is incorrect to interpret the layer of $Al_2O_3$ at 2 cycles as a layer of $Al_2O_3$ that results in the formation of a potential well and two-dimensional electron gas on the $ZnO|Al_2O_3$ interface. In addition, since the measurements were carried out in the air atmosphere, the near-surface region of ZnO is depleted due to adsorption of oxygen ions, and after application of aluminum oxide with a thickness of 0.2 nm the $ZnO|Al_2O_3$ interface most likely would be depleted due to adsorbed oxygen ions $O^-$.

Since Al is a dopant for ZnO, that is the substitution of $Zn^{2+}$ with $Al^{3+}$ in the crystalline lattice results in the situation when an Al atom acts as a donor of one electron, it is the doping of near-surface region of ZnO in the process of ALD-deposition of $Al_2O_3$ that can be considered as the main mechanism of the increase in electrical conductivity. This also matches the experimental data of producing

ZnO by ALD process with alternating the cycle of $Al_2O_3$ deposition and several cycles of ZnO deposition to achieve the pre-defined concentration of the dopants [8,31,39]. Also, the results of XPS demonstrate a shift of Zn2$p$ peak when depositing $Al_2O_3$ from the position of peak of the uncoated ZnO, a shift of Al2$p$ near the interface (at two cycles) from the position of Al2$p$ peak in the $Al_2O_3$ film (at 50 cycles), and a shift of the core level of oxygen with changing number of cycles of $Al_2O_3$ deposition. These shifts are indicative of electron interaction of atoms on the interface and confirm possible Incorporation of Al atoms into the crystal lattice of ZnO, that provides for the doping of zinc oxide. If the density of Al donors exceeds the critical Mott concentration (about $10^{19}$ for ZnO), then all Al donors are ionized even at a zero temperature, i.e., the semiconductor–metal transition takes place [39]. In our case with 2 cycles of $Al_2O_3$ deposition the percentage of Al atoms measured by XPS in the near-surface layer of the sample (at a depth of XPS-analysis $< 10$ nm) is $\sim 8.7\%$. If we assume, that all Al atoms substitute Zn atoms in the crystal lattice, the percentage of Zn atoms substituted for Al according to

$$\mathrm{AlF_{XPS}} = \frac{\mathrm{Al_{at\%}}}{\mathrm{Al_{at\%}} + \mathrm{Zn_{at\%}}} \cdot 100\%, \qquad (1)$$

should be 16.7%. The concentration of Zn ($n_{\mathrm{Zn}}$) in the hexagonal lattice of ZnO wurtzite is $4 \cdot 10^{22}\,\mathrm{cm}^{-3}$ [39]. Thus, the concentration of Al donors obtained from XPS, as defined by

$$n_{\mathrm{D}}^{\mathrm{XPS}} = \frac{\mathrm{AlF_{XPS}\%}}{100\%}\, n_{\mathrm{Zn}}, \qquad (2)$$

is $n_{\mathrm{D}}^{\mathrm{XPS}} \approx 6.7 \cdot 10^{21}\,\mathrm{cm}^{-3}$. The concentration of donors from XPS is considerably higher than that required for the Mott transition. The 6.7% percentage of Al atoms with two cycles of ALD process in the near-surface layer under analysis is also greater than the solubility limit of 2–3% for Al in ZnO films when Al can substitute Zn in the crystal lattice and act as a donor of electrons [40]. Even though in the case of the surface deposition of $Al_2O_3$ on ZnO solubility limit is a conditional concept, further shift of Al2$p$ peak with an increase in the number of cycles to a more oxidized form (to the peak in $Al_2O_3$) is indicative of the fact that, the most likely, the doping limit of the near-surface region and the Mott transition take place as early as at the first cycles of the $Al_2O_3$ deposition.

If the doping limit of the near-surface region is reached at the first cycles of the deposition, it is difficult to explain the $\sim$ 4-times increase in electrical conductivity with 5-times increase in the number of cycles and further $\sim$ 170-times increase in electrical conductivity in case of further 5-times increase in the number of cycles (from 10 to 50).

It is well known from literature, that oxide semiconductors contain on their surface a number of adsorption centers with different acidity [41–43]. Therefore, we assume, that due to adsorption centers with different energy parameters on the surface of the polycrystalline ZnO layer the growth of $Al_2O_3$ at a small number of cycles is not ideally conformal. That is the growth of $Al_2O_3$ film starts with the formation of clusters in the most energetically favorable centers. An increase in the number of cycles from 2 to 10 results in an increase in the regions of ZnO surface where $Al_2O_3$ is deposited and, respectively, the semiconductor–metal transition takes place. However, the regions of degenerate ZnO are still limited by undoped regions or regions doped to concentration values less than the Mott transition. At a certain number of cycles the conductive regions are joined together, that is a percolation cluster is formed and a sharp increase in electrical conductivity takes place. Verification of this assumption requires further studies.

It is worth noting, that the passivation of surface defects, such as oxygen vacancies and their complexes, on the ZnO surface with the atomic layer deposition of $Al_2O_3$ is likely as well. Nevertheless, we consider that in the studies where $Al_2O_3$ was deposited on ZnO to improve characteristics of multilayer structures, changes in characteristics of structures may be also connected to the doping of ZnO surface and redistribution of the space charge region between layers.

It is also worthy of note that the change in the electrical conductivity of nanorods or thin layers of ZnO in the air atmosphere with surface doping may be contributed by the screening of charges of adsorbed oxygen ions. The doped near-surface layer substitutes the charge carrier depleted near-surface layer.

## 4. Conclusion

In this study we have found an effect of sharp increase in the electrical conductivity of the system of ZnO nanorods upon the atomic layer deposition of $Al_2O_3$ on their surface. The XPS method was used to show that at 50 cycles of atomic layer deposition the $Al_2O_3$ conformally coats the surface of nanorods.

The study of thin films of ZnO after the atomic layer deposition of $Al_2O_3$ on the surface of ZnO with the variation of the number of cycles by methods of photoelectron spectroscopy has shown that the increase in the electrical conductivity of ZnO is connected to the electron interaction of atoms after $Al_2O_3$ deposition and, respectively, doping of the near-surface layer of ZnO. Also, we assume that the semiconductor–metal transition takes place during the first cycles of the atomic layer deposition of $Al_2O_3$, but the significant change in the electrical conductivity of the ZnO layer occurs when a percolation cluster is formed from conductive near-surface regions.

It is worth noting, that in many research reports the change in characteristics of structures under the deposition of $Al_2O_3$ on the surface of ZnO is associated with the passivation of surface defects, however, these changes may be contributed by the surface doping of ZnO with Al atoms.

The synthesis of nanostructured ZnO with different morphology and the possibility of surface doping of ZnO by means of the conformal atomic layer deposition of $Al_2O_3$

offers additional opportunities to produce nanostructured transparent electrodes of ZnO : Al.

### Funding

A.S. Komolov and E.F. Lazneva would like to thank the support of grant from the Russian Science Foundation No. 19-13-00021, https://rscf.ru/project/19-13-00021/, in the scope of which the samples were XPS-characterized. In this study the equipment of the Physical Methods of Surface Investigation center of the Research Park of Saint-Petersburg State University was used.

### Conflict of interest

The authors declare that they have no conflict of interest.

## References

[1] U. Ozgur, Y.I. Alivov, C. Liu, A. Teke, M.A. Reshchikov, S. Dogan, V. Avrutin, S.J. Cho, H.A. Morkoc. J. Appl. Phys. **98**, *4*, 041301 (2005).
[2] P.R. Brown, R.R. Lunt, N. Zhao, T.P. Osedach, D.D. Wanger, L.-Y. Chang, M.G. Bawendi, V. Bulovic. Nano Lett. **11**, *7*, 2955 (2011).
[3] A. Takahashi, H. Wang, T. Fukuda, N. Kamata, T. Kubo, H. Segawa. Energies **13**, *19*, 5037 (2020).
[4] D.S. Ahmed, B.K. Mohammed, M.K.A. Mohammed. J. Mater Sci **56**, *27*, 15205 (2021).
[5] L.-M. Wang, C.-Y. Wang, C.-R. Jheng, S.-J. Wu, C.-K. Sai, Y.-J. Lee, C.-Y. Chiang, B.-Y. Shew. Appl. Phys. A **122**, *8*, 731 (2016).
[6] L.M. Wong, S.Y. Chiam, W.K. Chim, J.S. Pan, S.J. Wang. Thin Solid Films **545**, 285 (2013).
[7] D.C. Look, K.D. Leedy, L. Vines, B.G. Svensson, A. Zubiaga, F. Tuomisto, D.R. Doutt, L.J. Brillson. Phys. Rev. B **84**, *11*, 115202 (2011).
[8] Y. Wu, P.M. Hermkens, B.W.H. van de Loo, H.C.M. Knoops, S.E. Potts, M.A. Verheijen, F. Roozeboom, W.M.M. Kessels. J. Appl. Phys. **114**, *2*, 024308 (2013).
[9] Y.-J. Lu, H.-F. Li, C.-X. Shan, B.-H. Li, D.-Z. Shen, L.-G. Zhang, S.-F. Yu. Opt. Express **22**, *14*, 7524 (2014).
[10] A. Rasool, M.C.S. Kumar, M.H. Mamat, C. Gopalakrishnan, R. Amiruddin. J. Mater. Sci.: Mater. Electron. **31**, *9*, 7100 (2020).
[11] M. Ding, D. Zhao, B. Yao, S.E.Z. Guo, L. Zhang, D. Shen. Opt. Express **20**, *13*, 13657 (2012).
[12] M. Willander, M.Q. Israr, J.R. Sadaf, O. Nur. Nanophotonics **1**, *1*, 99 (2012).
[13] V. Consonni, J. Briscoe, E. Kärber, X. Li, T. Cossuet. Nanotechnol. **30**, *36*, 362001 (2019).
[14] J. Al-Sabahi, T. Bora, M. Al-Abri, J. Dutta. Materials **9**, *4*, 238 (2016).
[15] S. Xu, Y. Qin, C. Xu, Y. Wei, R. Yang, Z.L. Wang. Nature Nanotechnol. **5**, *5*, 366 (2010).
[16] L.K. Krasteva, D.Ts. Dimitrov, K.I. Papazova, N.K. Nikolaev, T.V. Peshkova, V.A. Moshnikov, I.E. Grachyova, S.S. Karpova, N.V. Kaneva. FTP **47**, *4*, 564 (2013) (in Russian).
[17] A. Bobkov, A. Varezhnikov, I. Plugin, F.S. Fedorov, V. Trouillet, U. Geckle, M. Sommer, V. Goffman, V. Moshnikov, V. Sysoev. Sensors **19**, *19*, 4265 (2019).
[18] A.A. Ryabko, A.A. Bobkov, S.S. Nalimova, A.I. Maksimov, V.S. Levitsky, V.A. Moshnikov, E.I. Terukov. ZhTF **92**, *5*, 758 (2022) (in Russian).
[19] A.A. Ryabko, S.S. Nalimova, D.S. Mazing, O.A. Korepanov, A.M. Guketlov, O.A. Aleksandrova, A.I. Maksimov, V.A. Moshnikov, Z.V. Shomakhov, A.N. Alyoshin. ZhTF **92**, *6*, 845 (2022) (in Russian).
[20] A.B. Nikol'skaya, S.S. Kozlov, M.F. Vil'danova, O.I. Shevaleevsky. FTP **53**, *4*, 550 (2019) (in Russian).
[21] S. Zang, Y. Wang, W. Su, H. Zhu, G. Li, X. Zhang, Y. Liu. Phys. Status Solidi RRL **10**, *10*, 745 (2016).
[22] S. Ozu, Y. Zhang, H. Yasuda, Y. Kitabatake, T. Toyoda, M. Hirata, K. Yoshino, K. Katayama, S. Hayase, R. Wang, Q. Shen. Frontiers. Energy Res. **7**, 11 (2019).
[23] B. Wei, Z. Tang, S. Wang, C. Qing, C. Li, X. Ding, Y. Gao, X. Portier, F. Gourbilleau, D. Stiévenard, T. Xu. Nanotechnol. **29**, *39*, 395204 (2018).
[24] S. Zang, Y. Wang, M. Li, W. Su, M. An, X. Zhang, Y. Liu. Chin. Phys. B **2**, *1*, 018503 (2018).
[25] K.R. Nandanapalli, D. Mudusu. ACS Appl. Nano Mater. **1**, *8*, 4083 (2018).
[26] K. Gawlinska-Necek, M. Wlazlo, R. Socha, I. Stefaniuk, L. Major, P. Panek. Materials **14**, *4*, 1038 (2021).
[27] H.-Y. Chen, H.-L. Lu, L. Sun, Q.-H. Ren, H. Zhang, X.-M. Ji, W.-J. Liu, S.-J. Ding, X.-F. Yang, D.W. Zhang. Sci. Rep. **6**, 38486 (2016).
[28] D. Garcia-Alonso, S. Smit, S. Bordihn, W.M.M. Kessels. Semicond. Sci. Technol. **28**, *8*, 082002 (2013).
[29] B. Min, J.S. Lee, J.W. Hwang, K.H. Keem, M.I. Kang, K. Cho, M.Y. Sung, S. Kim, M.-S. Lee, S.O. Park, J.T. Moon. J. Crystal Growth **252**, *4*, 565 (2003).
[30] M. Steglich, A. Bingel, G. Jia, F. Falk. Solar Energy Mater. Solar Cells **103**, 62 (2012).
[31] K. Zhao, J. Xie, Y. Zhao, D. Han, Y. Wang, B. Liu, J. Dong. Nanomater. **12**, *2*, 172 (2022).
[32] A.A. Ryabko, A.I. Maksimov, V.N. Verbitsky, V.S. Levitsky, V.A. Moshnikov, E.I. Terukov. FTP **54**, *11*, 1251 (2020) (in Russian).
[33] A. Komolov, K. Schaumburg, P.J. Moller, V.V. Monakhov. Appl. Surf. Sci. **142**, *1–4*, 591 (1999).
[34] J. Joo, B.Y. Chow, M. Prakash, E.S. Boyden, J.M. Jacobson. Nature Mater. **10**, *8*, 596 (2011).
[35] S. Iaiche, A. Djelloul. J. Spectroscopy **2015**, 836859 (2015).
[36] H.H.-Ch. Lai, T. Basheer, V.L. Kuznetsov, R.G. Egdell, R.M.J. Jacobs, M. Pepper, P.P. Edwards. J. Appl. Phys, **112**, *8*, 083708 (2012).
[37] S. Wu, M.-Y. Lin, S.-H. Chang, W.-C. Tu, C.-W. Chu, Y.-C. Chang. J. Phys. Chem. C **122**, *1*, 236 (2018).
[38] J. Yang, B.S. Eller, M. Kaur, R.J. Nemanich. J. Vacuum Sci. Technol. A **32**, *2*, 021514 (2014).
[39] A. Mošková, M. Moško, M. Precner, M. Mikolášek, A. Rosová, M. Mičušík, V. Štrbík, J. Šoltýs, F. Gucmann, E. Dobročka, K. Fröhlich. J. Appl. Phys. **130**, *3*, 035106 (2021).
[40] R.E. Vesto, R. Wilson, H. Choi, K. Kim. AIP Advances **10**, *9*, 095211 (2020).
[41] S.S. Karpova, V.A. Moshnikov, S.V. Myakin, E.S. Kolovangina. FTP **47**, *3*, 369 (2013) (in Russian).
[42] S.S. Karpova, V.A. Moshnikov, A.I. Maksimov, S.V. Myakin, N.E. Kazantseva. FTP **47**, *8*, 1022 (2013) (in Russian).
[43] I.A. Pronin, N.D. Yakushova, I.A. Averin, A.A. Karmanov, A.S. Komolov, M.M. Sychyov, V.A. Moshnikov, E.I. Terukov. Neorgan. materialy **57**, *11*, 1207 (2021) (in Russian).